

# Streamflow indices to identify catchment drivers of hydrograph

Formatted: Centered

Jeenu Mathai<sup>1</sup> and Pradeep P. Mujumdar<sup>1,2</sup>

<sup>1</sup>Department of Civil Engineering, Indian Institute of Science, Bangalore, India

<sup>2</sup>Interdisciplinary Centre for Water Research, Indian Institute of Science, Bangalore, India

Correspondence to: Pradeep P. Mujumdar ([pradeep@iisc.ac.in](mailto:pradeep@iisc.ac.in))

**Abstract.** Streamflow indices are flow descriptors that quantify the streamflow dynamics, which are usually determined for a specific basin and are distinct from other basin features. The ~~streamflow indices~~ ~~flow descriptors~~ are appropriate for large-scale and comparative hydrology studies, independent of statistical assumptions and can distinguish signals that indicate basin behavior over time. In this paper, the characteristic features of the hydrograph's temporal asymmetry due to its different underlying hydrologic processes are primarily highlighted.

~~Time irreversibility/ or temporal asymmetry refers here to the steeper ascending and gradual descending parts of a streamflow hydrograph.~~ Streamflow indices linked to each limb of the hydrograph within the time-irreversibility paradigm are distinguished with respect to its processes driving the rising and falling limbs. -Various streamflow indices relating the rising and falling limbs, and the catchment attributes such as climate, topography, vegetation, geology and soil are then correlated. Finally, the key attributes governing rising and falling limbs are identified. The novelty of the work is on differentiating hydrographs by their time irreversibility property and offering an alternative way to recognize primary drivers of streamflow hydrographs. A set of streamflow indices at the catchment scale for 671 basins in the Contiguous United States (CONUS) is ~~presented-introduced~~ here. These streamflow indices complement the catchment attributes provided earlier (Addor et al., 2017) for the CAMELS data set. A series of spatial maps describing the streamflow indices and their regional variability over the CONUS is illustrated in this study.

## 1 Introduction

Hydrologists use data to ~~understand~~ ~~underpin~~ the hydrologic system by identifying several unique catchment signatures and employ various flow descriptors independent of statistical assumptions yet capable of capturing signals that reflect the basin's long-term unique behavior. Hydrological indices, commonly referred to as hydrologic metrics, hydrologic signatures, or diagnostic signatures, are quantitative flow metrics that characterize statistical or dynamical hydrological data series (McMillan, 2021). Specifically, streamflow indices are flow descriptors derived from discharge time-series data, and a considerable collection of indices are available to aid in the better characterization of hydrological features, ranging from basic statistics like the mean to more sophisticated metrics (Addor et al., 2018; McMillan, 2021). In many cases, daily streamflow records are not permitted for redistribution; however, researchers have computed streamflow indices and made them publicly accessible.

37  
38  
39  
40  
41  
42  
43  
44  
45  
46  
47  
48  
49  
50  
51  
52  
53  
54  
55  
56  
57  
58  
59  
60  
61  
62  
63  
64  
65  
66  
67  
68  
69  
70

Hydrological indices are increasingly used in emerging areas such as global-scale hydrologic modeling and large-sample hydrology to extract relevant information and compare the different watershed processes (Addor et al., 2017, 2018; McMillan, 2021). These indices offer an indirect way to explore hydrological processes as well as provide insights into hydrologic behavior in catchments where data other than streamflow is restricted and are widely used in process exploration, model calibration, model selection, and catchment classification (Addor et al., 2018; Clark et al., 2011; Kuentz et al., 2017; McMillan et al., 2011; Sawicz et al., 2011). McMillan (2021) presented a classification that differentiates between statistics- and dynamics-based signatures and between signatures at different timescales.

The relevance of time irreversibility (or temporal asymmetry) of streamflow variability on a daily scale has been emphasized in recent studies (Koutsoyiannis, 2020; Mathai and Mujumdar, 2019; Serinaldi and Kilsby, 2016). The disparity in physical mechanisms driving the hydrograph's ~~ascension-rising~~ and ~~falling recession~~-limbs (Fig.1) contributes to time irreversibility. Unlike other variables such as temperature, wind, precipitation, time irreversibility has been marked for streamflow at a daily scale (Koutsoyiannis, 2020). Streamflow recessions convey valuable information about the basin storage properties and aquifer characteristics (Aksoy & Bayazit, 2000). High variability encountered in the recession behaviour of individual segments is always a challenge in modeling the recession limb (Tallaksen, 1995). Recessions do not follow a simple form, due to their nonlinear nature (Aksoy et al., 2001). Various segments of recession represent different stages in the flow process and there is a need to differentiate the recession to various segments and to characterize the recession rates separately. Moreover, the various segments of the recession phase represent different phases in the flow process. As a result, time irreversibility must be acknowledged in streamflow analysis, accounting for the distinction of the recession into different segments, with a faster recession induced by high discharges caused by surface runoff and a slower recession caused by baseflow (Fig.1), and the characterization of the recession rates separately (Mathai and Mujumdar, 2019). In this study, streamflow indices are chosen to better understand different hydrological processes by recognizing the streamflow hydrograph's temporal asymmetry. Theis work's main novelty of this work is to differentiate hydrographs by their time irreversibility property and using their associated indices by offering an alternative way to recognize primary drivers of streamflow hydrographs. This work's main novelty in the work presented here -is to differentiate hydrograph limbs by their time irreversibility property and use their associated indices to provide an approach to derive insights on the primary drivers of streamflow hydrographs.

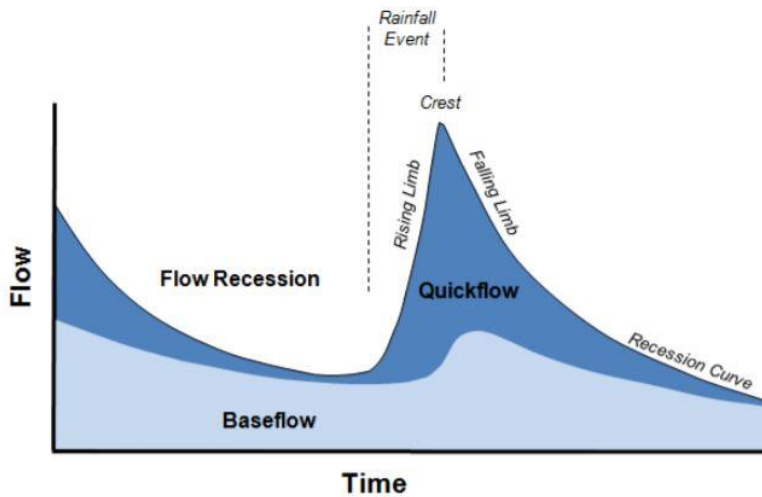


**Figure 1.** Schematic representation of rising limb and falling limb  
(source: Environment Southland;

<https://www.es.govt.nz/environment/water/groundwater/groundwater-monitoring>)

71  
72  
73  
74  
75  
76  
77  
78  
79  
80  
81  
82  
83  
84  
85  
86  
87  
88  
89  
90  
91  
92  
93  
94  
95  
96  
97

The analysis employs a collection of indices drawn from hydrograph shape diagnoses, to which extracts information about a basin's the properties of rising and falling limbs' inherent properties of the hydrograph. The principle of time irreversibility is encapsulated by six streamflow indices that describe and characterize at the shape of a streamflow hydrograph's shape.

Formatted: Indent: Left: 0 cm

The goals of this study are as follows: i) to identify the key drivers of streamflow hydrograph (rising and falling limbs) in terms of catchment attributes (eg. mean slope, aridity, fraction of precipitation falling as snow) using time-irreversibility-based indices ii) to present a spatial map-based attribute class based on streamflow-of indices to address used indices for a large-sample hydrology dataset. The attribute class is a broad classification of attributes based on a particular aspect/feature. Topography, climate, and soil are examples of attribute classes. In this study, we present a new attribute class of streamflow indices related to rising and falling limbs, referred to as "TI-streamflow indices" (Time-irreversibility streamflow indices).

Formatted: Font: Not Bold, Not Italic

Formatted: Font: Not Bold

Hydrograph analysis is referred to as called as the investigation of the numerous factors that influence hydrograph shape (Rogers, 1972). The presence of hydrographs with a similar shape in long-term observation series of water runoff demonstrates that the same conditions of water runoff generation reoccur from time to time in the catchment of a river due to climate cyclicity and as a result of hydrological processes (Khrystyuk et al., 2017). Because climatic factors are dynamic in space and time, they seem to be the most significant factors influencing the hydrograph shape (Khrystyuk et al., 2017). Temperature, snow water equivalent, and snowmelt conditions are the most critical factors influencing the shape of hydrographs (Khrystyuk et al., 2017). The shape, timing, and peak flow of a streamflow hydrograph are influenced spatially and temporally by rainfall and watershed factors (Singh, 1997). Using a physical laboratory model, a study has investigated the influence of chosen meteorological and physiographic parameters on the runoff hydrograph (Roberts and Klingeman, 1970). Storm-related parameters (rainfall intensity, rainfall duration, storm movement) and basin surface conditions are among the inputs that could

Formatted: Space After: 8 pt, Line spacing: 1.5 lines

98 be experimentally modified in the model (simulated permeability, antecedent moisture conditions). The study  
99 revealed that each variable was shown to have a substantial impact on the shape of the hydrograph (Roberts and  
100 Klingeman, 1970). Certain factors had a more considerable impact on the rising limb of the runoff hydrograph,  
101 whereas others were more important in terms of the flood crest (Roberts and Klingeman, 1970).

Formatted: Font: 10 pt, Not Bold, Font color: Auto, English (United States)

102 As shown in numerous ways/studies in the literature, our notion of time-irreversibility and its indices could also  
103 perform ~~de~~ a reasonable job of articulating the catchment drivers of streamflow hydrographs. This study presents  
104 an attribute class of hydrograph shape descriptors with temporal asymmetry. The significance of large-sample  
105 hydrology datasets in open hydrologic science and their potential to improve hydrological studies' transparency is  
106 also underlined in this study.

Formatted: Indent: Left: 0 cm

107 Large-sample hydrology (LSH) gathers information from a large~~er~~ number of catchments to gain a more  
108 comprehensive understanding of hydrological processes and to go beyond individual case studies. LSH helps  
109 identify catchment behavior and leads one to derive precise conclusions regarding different hydrological  
110 processes and models (Addor et al., 2020). Studies involving large-sample catchments help in understanding the  
111 drivers of hydrological change (Blöschl et al., 2019), in assessing hydrological similarity and classification  
112 (Berghuijs et al., 2014; K. A. Sawicz et al., 2014), in predictions in ungauged basins (Ehret et al., 2014), and in  
113 analysing model and data uncertainty (Coxon et al., 2014) and foster hydrology research by standardizing and  
114 automating the creation of large-sample hydrology datasets worldwide (Addor et al., 2020). LSH assists in  
115 exploring interrelationships between numerous catchment attributes related to landscape, climate, and hydrology  
116 (Addor et al., 2017; Alvarez-Garreton et al., 2018; Gupta et al., 2014; Newman et al., 2015; Sawicz et al., 2011)  
117 and generalizing rules that can significantly improve the predictability of the water cycle (Alvarez-Garreton et al.,  
118 2018).

119 The primary challenges in fostering LSH are data availability and accessibility, which seriously hinder its use in  
120 data-scarce regions. Despite the fact that a few large-scale hydrology studies have been undertaken, the number  
121 of publicly available large-scale datasets is still restricted (Addor et al., 2017, 2020; Coxon et al., 2020). Moreover,  
122 licensing restrictions and strict access policies make the datasets rarely available to the public (Coxon et al., 2020).

123 Model Parameter Estimation Experiment project (MOPEX) dataset (Duan et al., 2006), Canadian model parameter  
124 experiment (CANOPEX) database (Arsenault et al., 2016), Global Streamflow Indices and Metadata Archive (Do  
125 et al., 2018; Gudmundsson et al., 2018), Global Runoff Reconstruction (Ghiggi et al., 2019), HydroATLAS (Linke  
126 et al., 2019) and the Catchment Attributes and MEteorology for Large-Sample studies (CAMELS) (Addor et al.,  
127 2017) are notable contributions of open and accessible large-sample catchment datasets (Coxon et al., 2020). The  
128 concept of time irreversibility-based streamflow indices is then applied to CAMELS catchments with the goal of  
129 encouraging large-sample hydrology studies.

Formatted: Font: Not Bold, English (India)

## 130 **2 Methods**

131 To facilitate a comprehension of various hydrological processes and streamflow hydrograph drivers, the study  
132 employs streamflow indices considering the streamflow hydrograph's temporal asymmetry. The description of  
133 indices used in this study are tabulated in Table 1. Streamflow indices linked to each limb of the streamflow  
134 hydrograph within the time-irreversibility paradigm are distinguished since hydrographs have rising and falling  
135 limbs. The following indices are considered in the rising limb category: 1) rising limb density, 2) rising limb shape

136 parameter, and 3) rising limb scale parameter. In contrast, 1) falling limb density 2) slope of upper recession  
 137 (upper recession coefficient) 3) slope of lower recession (lower recession coefficient) are selected in falling limb  
 138 category. The next step is to compute these indices for a large number of catchments and correlate them with  
 139 attributes such as climate, topography, vegetation, geology, and soil. The streamflow indices can be correlated  
 140 explicitly since sub-categories are involved in each of the catchment attributes discussed above. Finally, the key  
 141 attributes governing ~~rising ascension~~ and ~~falling recession~~ limbs can be summarized and identified. ~~This work's~~  
 142 ~~main novelty is to differentiate hydrographs by their time irreversibility property and using their associated indices~~  
 143 ~~by offering an alternative way to recognize primary drivers of streamflow hydrographs.~~ The specifics of indices  
 144 are explained further below.

145 Rising limb density (RLD) is defined as the ratio of the number of rising limbs and the cumulative time of rising  
 146 limbs (Shamir et al., 2005). RLD is a hydrograph shape descriptor without considering the flow magnitude (Fig.  
 147 2) and the expression for RLD is given as,

$$RLD = \frac{N_{RL}}{T_R} \quad (1)$$

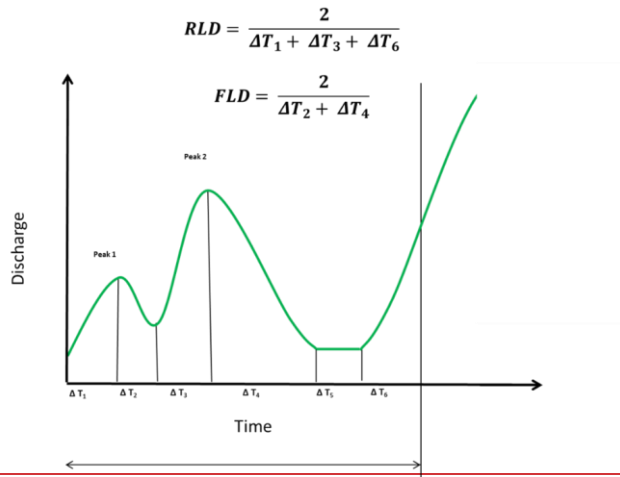
148 The ratio of the number of falling limbs to the cumulative time of falling limbs is termed as falling limb density  
 149 (FLD) (Fig. 2) (Shamir et al., 2005). The expression for FLD is given as,

$$FLD = \frac{N_{FL}}{T_F} \quad (2)$$

150 **Table 1.** Hydrological descriptors with temporal asymmetry.

Sl.no	Attribute	Description	Unit	Data source	References
1	RLD	Rising limb density	day <sup>-1</sup>	N15—USGS data	Shamir et al. (2005)
2	FLD	Falling limb density	day <sup>-1</sup>		
3	a	ascension limb scale parameter	-		Mathai and Mujumdar, (2019)
4	b	ascension limb shape parameter	-		
5	b <sub>u</sub>	Upper recession coefficient	-		
6	b <sub>l</sub>	Lower recession coefficient	-		

151



152  
153 **Figure 2.** Schematic example of rising limb density (RLD) and falling limb density (FLD) calculation  
154 (Shamir et al., 2005).

155 The diurnal increments of streamflow are fitted with an appropriate probability density function to depict  
156 the shape of the ascension limbs which occur on wet days. The Weibull distribution reflects the diurnal  
157 increments of streamflow that occur on wet days reasonably well (Mathai and Mujumdar, 2019; Stagge  
158 and Moglen, 2013; Szilagyi et al., 2006), and the scale ‘ $\alpha$ ’ and shape ‘ $b$ ’ parameters of the Weibull  
159 distribution are computed for each catchment by using observed diurnal increments of streamflow. In  
160 contrast, an exponential recession is used to capture the shape of the recession limbs on dry days of the  
161 daily hydrograph, representing the falling limbs' underlying dynamics (Mathai and Mujumdar, 2019). As  
162 the upper recession refers to the fast flow following a storm event and the lower recession refers to the  
163 baseflow recession, falling limb modeling is done in two stages.

164 The study uses indices related to ascension limb (viz., RLD, ascension limb scale parameter, ascension limb shape  
165 parameter) and recession limb (viz., FLD, upper recession coefficient, lower recession coefficient) to summarize  
166 the characteristic shape of steeper rising and gradually declining falling limb and its application in understanding  
167 the role of various drivers of catchment attributes in streamflow generation. Table 1. Hydrological descriptors  
168 with temporal asymmetry.

169

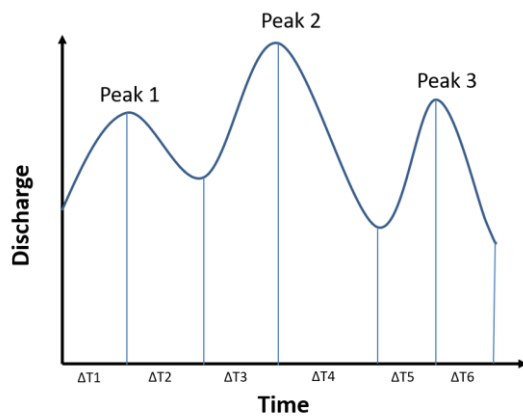
<i>Attribute</i>	<i>Description</i>	<i>Unit</i>	<i>Data source</i>	<i>References</i>
<i>Rising limb</i>	RLD	Rising limb density	$\text{day}^{-1}$	Shamir et al. (2005)
	a	Rising limb scale parameter	=	Mathai and Mujumdar, (2019)
	b	Rising limb shape parameter	=	Mathai and Mujumdar, (2019)
<i>Falling limb</i>	FLD	Falling limb density	$\text{day}^{-1}$	Shamir et al. (2005)
	$b_1$	Upper recession coefficient	=	Mathai and Mujumdar, (2019)

	$b_2$	Lower recession coefficient	=		Mathai and Mujumdar, (2019)
--	-------	-----------------------------	---	--	-----------------------------

170

$$\text{Rising limb density} = \frac{3}{\Delta T1 + \Delta T3 + \Delta T5}$$

$$\text{Falling limb density} = \frac{3}{\Delta T2 + \Delta T4 + \Delta T6}$$



171

172 **Figure 2.** Schematic example of rising limb density (RLD) and falling limb density (FLD) calculation (Shamir et  
 173 al., 2005).

174 We first identify the hydrologic state of the stream (ascension and recession) (Mathai and Mujumdar, 2019). To  
 175 determine the hydrologic state of a stream - increasing (wet) or decreasing (dry) - on a given day, a time series of  
 176 diurnal increments is extracted by differencing the original time series with its one-day lagged time series. The  
 177 positive increments are identified as diurnal increments for wet days (ascension limb).

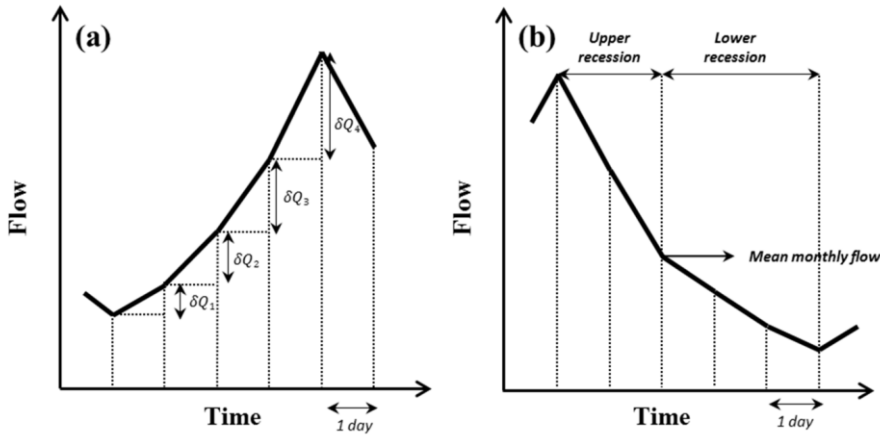


**Figure 3.** Schematic representation of flow series (a) ascension limb and (b) recession limb (Mathai and Mujumdar, 2019).

To characterize the shape of the rising limbs occurring on wet days, the diurnal increments are fitted using an appropriate probability density function. The Weibull distribution reflects the diurnal increments of streamflow that occur on wet days satisfactorily (Mathai and Mujumdar, 2019; Stagge and Moglen, 2013; Szilagyi et al., 2006), and the scale 'a' and shape 'b' parameters of the Weibull distribution are computed for each catchment by using observed diurnal increments of streamflow (indicating  $\delta Q$ ) of the ascension limb (Fig 3.a). The Weibull pdf is positive only for positive values of  $x$ , and is zero otherwise. For strictly positive values of the scale parameter  $a$  and shape parameter  $b$ , the density function is given by

$$f(x; a, b) = \begin{cases} \frac{b}{a} \left(\frac{x}{a}\right)^{b-1} e^{-(x/a)^b} & x \geq 0, \\ 0 & x < 0, \end{cases} \quad (3)$$

where  $a > 0$ ,  $b > 0$ . The shape and scale parameters of the Weibull distribution are estimated for each catchment from the observed diurnal increments of the streamflow. The scale parameter controls the magnitude of the increasing limb, whilst the shape parameter reflects the flashiness of the increasing limb. The scale parameter is related to the magnitude of storm events which mirrors the general shape of flows in the stream. As a result, correlating these parameters with catchment attributes reveals which catchment attributes drive the magnitude and flashiness of rising limbs.

In contrast, an exponential recession is used to capture the shape of the falling limbs on dry days of the daily hydrograph, representing the falling limbs' underlying dynamics (Mathai and Mujumdar, 2019). As the upper recession refers to the fast flow following a storm event and the lower recession refers to the baseflow recession, falling limb modeling is done in two stages (Fig 3.b) (Aksoy, 2003; Aksoy and Bayazit, 2000). The steps to obtain recession coefficients  $b_1$  and  $b_2$  are explained below (Mathai and Mujumdar, 2019). To portray the shape of the recession limbs occurring on dry days of the daily hydrograph, an exponential recession is employed to capture the falling limbs' underlying dynamics (Mathai & Mujumdar, 2019). The expression for the exponential recession is given as follows.

Formatted: Font: Bold

Formatted: Line spacing: 1.5 lines



$$Q_t = Q_0 e^{-bt} \quad (4)$$

202 where  $b$  is the recession coefficient,  $t$  is time,  $Q_t$  is the flow  $t$  days after the peak and  $Q_0$  is the peak flow (Mathai  
203 & Mujumdar, 2019). Mean flow value is chosen as an appropriate measure (Sargent, 1979) to divide the recession  
204 into two stages. The limbs with a peak flow value greater than the observed mean flow value are considered as  
205 upper recessions and those with peak flow values smaller than the observed mean as lower recessions. The upper  
206 recession is modelled as follows,

$$Q_t = Q_0 e^{-b_1 t} \quad (5)$$

207 where  $b_1$  is the recession coefficient for the upper part of the recession limb,  $t$  is the number of days after the  
208 peak,  $Q_t$  is flow  $t$  days after the peak,  $Q_0$  is the preceding peak flow (Mathai & Mujumdar, 2019). The lower  
209 recession is represented as,

$$Q_t = Q_0^* e^{-b_2(t-t^*)} \quad (6)$$

210 where  $b_2$  is the recession coefficient for the lower part of the recession limb,  $t^*$  is the time from the start of the  
211 lower recession,  $Q_0^*$  is the initial flow in the lower part of the recession (Mathai & Mujumdar, 2019). The recession  
212 expressions for upper and lower recession are fitted by regressing  $\ln(Q_t/Q_0)$  versus  $t$  and  $\ln(Q_t/Q_0^*)$  versus  $t -$   
213  $t^*$  respectively. These linear regressions are performed on each individual recession sequence. The average of the  
214 upper/lower recession parameters is taken as the upper/lower recession parameter of that catchment (on daily time  
215 series data).

216 The study uses indices related to rising limb (viz., RLD, rising limb scale parameter, rising limb shape parameter)  
217 and recession limb (viz., FLD, upper recession coefficient, lower recession coefficient) to summarize the  
218 characteristic shape of steeper rising and gradually declining falling limb and its application in understanding the  
219 role of various drivers of catchment attributes in streamflow generation.

220

### 221 **3-Contributions of the Study**

222 The analysis employs a collection of indices drawn from hydrograph shape diagnoses, which extracts information  
223 about a basin's ascension and recession limbs' inherent properties. The principle of time irreversibility is  
224 encapsulated by six streamflow indices that describe and characterize a streamflow hydrograph's shape, and  
225 indices for a particular basin are consistent and distinct from indices from other basins.

226 The goals of this study are as follows: i) to identify the key drivers of streamflow hydrographs (in terms of  
227 catchment attributes) using time irreversibility-based indices ii) to present a spatial map-based attribute class of  
228 time-irreversibility-based indices for a large sample hydrology dataset.

229 As shown in numerous ways/studies in the literature, our notion of time irreversibility and its indices could also  
230 do a reasonable job of articulating the catchment drivers of streamflow hydrographs. This study presents an  
231 attribute class of hydrograph shape descriptors with temporal asymmetry. The significance of large sample

Formatted: Indent: Left: 0 cm

hydrology datasets in open hydrologic science and their potential to improve hydrological studies' transparency is also underlined in this study.

#### 4 Motivation to extend to large sample hydrology

Large sample hydrology (LSH) gathers information from a larger number of catchments to gain a more comprehensive understanding of hydrological processes and to go beyond individual case studies. LSH helps identify catchment behavior and leads one to derive precise conclusions regarding different hydrological processes and models (Addor et al., 2020). Studies involving large sample catchments help in understanding the drivers of hydrological change (Blöschl et al., 2019), in assessing hydrological similarity and classification (Berghuijs et al., 2014; K. A. Sawicz et al., 2014), in predictions in ungauged basins (Ehret et al., 2014), and in analysing model and data uncertainty (G. Coxon et al., 2014) and foster hydrology research by standardizing and automating the creation of large sample hydrology datasets worldwide (Addor et al., 2020). LSH assists in exploring interrelationships between numerous catchment attributes related to landscape, climate, and hydrology (Addor et al., 2017; Alvarez Garreton et al., 2018; Gupta et al., 2014; Newman et al., 2015; K. Sawicz et al., 2011) and generalizing rules that can significantly improve the predictability of the water cycle (Alvarez Garreton et al., 2018).

The primary challenges in fostering LSH are data availability and accessibility, which seriously hinder its use in data scarce regions. Despite the fact that a few large scale hydrology studies have been undertaken, the number of publicly available large scale datasets is still restricted (Addor et al., 2017, 2020; Coxon et al., 2020). Moreover, licensing restrictions and strict access policies make the datasets rarely available to the public (Coxon et al., 2020).

Model Parameter Estimation Experiment project (MOPEX) dataset (Duan et al., 2006), Canadian model parameter experiment (CANOPEX) database (Arsenault et al., 2016), Global Streamflow Indices and Metadata Archive (Do et al., 2018; Gudmundsson et al., 2018), Global Runoff Reconstruction (Ghiggi et al., 2019), HydroATLAS (Linke et al., 2019) and the Catchment Attributes and MEteorology for Large Sample studies (CAMELS) (Addor et al., 2017) are notable contributions of open and accessible large sample catchment datasets (Coxon et al., 2020).

Addor et al. (2017) introduced a new dataset (CAMELS) made publicly available for large sample hydrological studies. This dataset covers meteorological and streamflow datasets provided by Newman et al. (2015) and provides quantitative metrics for a large variety of attributes for 671 catchments in the contiguous United States (CONUS). Streamflow records are available in the dataset from 1990 to 2009 for the 671 catchments, which are minimally influenced by human activities (Addor et al., 2017).

The CAMELS dataset prompted hydrological research by enabling open access to hydrologic data and establishing a common standard across the database. CAMELS promoted open access to datasets for the United States, and it is eventually expanded to the United Kingdom (CAMELS-GB), Chile (CAMELS-CL), and Brazil (CAMELS-BR). The CAMELS proposes five classes of catchment attributes, namely location, topography, geology, land cover characteristics, climatic indices, and hydrological signatures, in order to promote common standards and formats in large sample studies (Addor et al., 2017). The concept of time irreversibility based streamflow indices is then applied to CAMELS catchments with the goal of encouraging large sample hydrology studies.

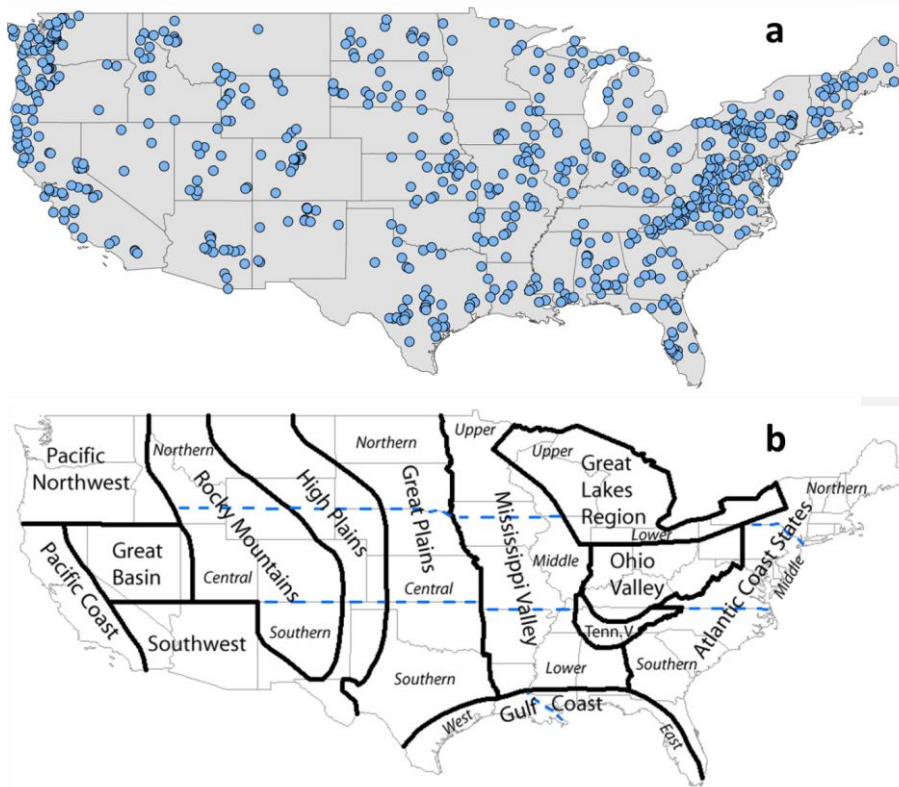
#### 3.5 Dataset used

270 Section 35 provides the description of the dataset used and the study area chosen. This study employs the  
 271 CAMELS dataset, which encompasses daily discharge data and catchment attributes for 671 catchments (Fig. 43)  
 272 across the continental United States, representing a diverse set of catchments with long streamflow time series  
 273 covering a wide range of hydro-climatic conditions (Addor et al., 2017). The time frame chosen for the analysis  
 274 is from 1 October 1989 to 30 September 2009 (Addor et al., 2017).

275 The topographic characteristics of CAMELS dataset are represented in Fig. S14. Except for the Appalachian  
 276 Mountains, the eastern part of the Continental United States is much flatter than the western portion, according to  
 277 mean elevation and mean slope maps (Fig. S14.a and S14.b). Figure S14.c depicts the spatial pattern of catchment  
 278 size, highlighting presence of some catchments with an area greater than 10,000 km<sup>2</sup>. The landscape of each  
 279 catchment is described using multiple attributes, which can be divided into various classes as shown in Table S12  
 280 (Addor et al., 2017). The details of the attributes used in this study is summarized in Table 2.

281  
 282  
 283

- Formatted: Not Highlight
- Formatted: Indent: Left: 0 cm, Line spacing: 1.5 lines
- Formatted: Not Highlight
- Formatted: Not Highlight
- Formatted: Not Highlight
- Formatted: Indent: Left: 0 cm

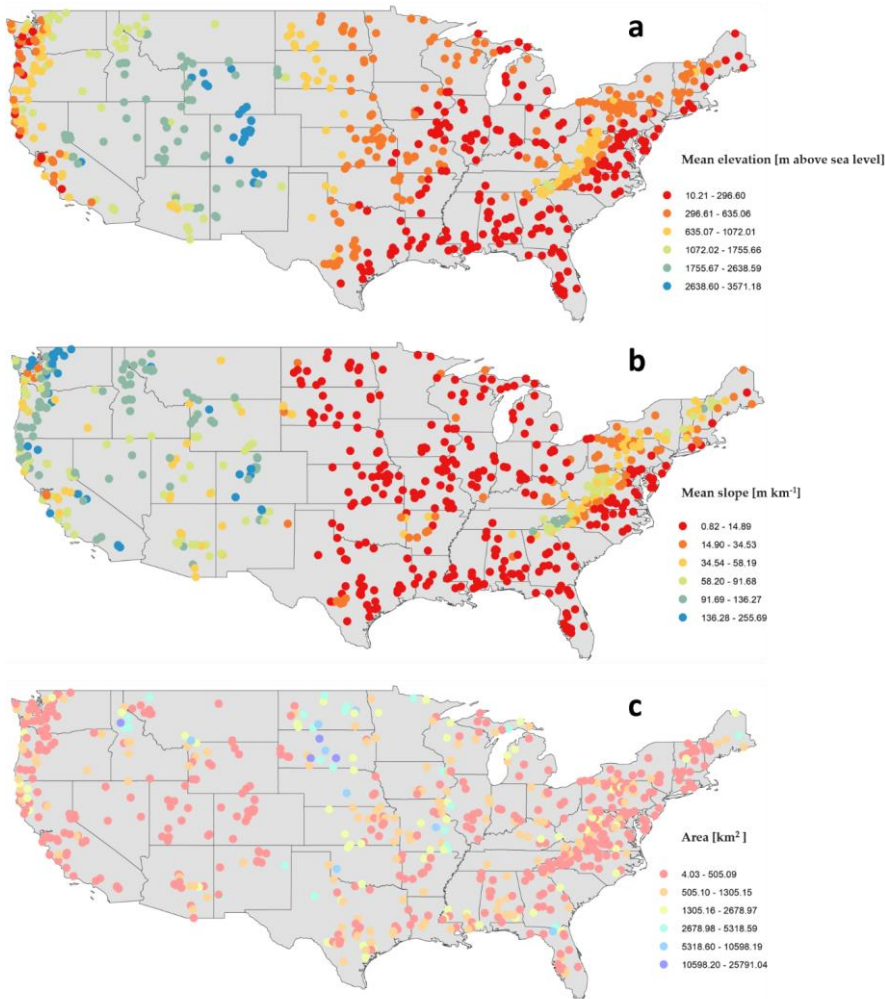


284

285 **Figure 43.** (a) Map of 671 CAMELS catchments in the continental United States considered in this study. (b)  
286 Geographical regions of US according to NOAA National Centers for Environmental Information referred for the  
287 analysis (source: NOAA National Centers for Environmental Information; <https://www.ncdc.noaa.gov/temp-and-precip/drought/nadm/geography>).  
288

Formatted: Indent: Left: 0 cm

289



290

291

292 **Figure 4.** Maps of topographic characteristics of CAMELS catchments over the CONUS (Addor et al., 2017):  
293 (a) Mean elevation [m above sea level] (b) Mean slope [m km<sup>-1</sup>] (c) Area [km<sup>2</sup>]. The eastern US seems to have a  
294 much flatter mean elevation and mean slope than the western US, which significantly influences catchment  
295 behavior. The majority of the catchments are noticed to be smaller, with an area of fewer than 3000 km<sup>2</sup>.

296

297

298  
299  
300  
301  
302  
303  
304

### 5.1 Catchment attributes

The landscape of each catchment is described using multiple attributes, which can be divided into various classes as shown in Table 2 (Addor et al., 2017). The details of the attributes used in this study is summarized in Table 2.

**Table 2.** CAMELS attributes (Addor et al., 2017)

Sl.no	Attribute	Description	Unit
<b>Climatic indices</b>			
1	aridity	aridity (ratio of mean PET to mean precipitation)	-
2	p_seasonality	seasonality and timing of precipitation (positive (negative) values indicate that precipitation peaks in summer (winter); values close to 0 indicate uniform precipitation throughout the year)	-
3	frac_snow	fraction of precipitation falling as snow	-
4	high_prec_freq	frequency of high precipitation days	days yr <sup>-1</sup>
5	high_prec_dur	average duration of high precipitation events	days
6	low_prec_freq	frequency of dry days	days yr <sup>-1</sup>
7	low_prec_dur	average duration of dry periods	days
<b>Land-cover characteristics</b>			
8	Forest_frac	forest fraction	-
9	Lai_max	maximum monthly mean of the leaf area index	-
10	Gvf_max	maximum monthly mean of the green vegetation fraction	-
<b>Soil characteristics</b>			
11	soil_depth_pelletier	depth to bedrock	m
12	sand_frac	sand fraction	%
13	clay_frac	clay fraction	%
<b>Geological characteristics</b>			

14	geol_porosity	subsurface porosity	-
15	geol_permeability	subsurface permeability (log10)	m <sup>2</sup>

307

305  
306  
308  
309  
310  
311  
312  
313  
314  
315  
316  
317  
318  
319  
320  
321  
322  
323  
324  
325  
326  
327  
328  
329  
330  
331  
332  
333  
334  
335  
336

#### 46 Results and Discussion

The first sub-section below looks at the regional variability of the streamflow indices used in this study. For the 671 CAMELS catchments, rising limb density, falling limb density, [rising recession](#) limb scale parameter, [rising recession](#) limb shape parameter, upper recession coefficient, and lower recession coefficient are computed and given as spatial maps. Streamflow indices are then presented in hydrological clusters to incorporate a more explicit spatial representation of catchment behavior across the CONUS. Catchment attributes cover a broad range of aspects of catchment hydrology such as, land cover, soil, climate, geology, topography and the association between these attributes and streamflow indices is discussed further in the subsequent section. As the climate is the most important factor in the US for the hydrological behavior for the CAMELS dataset (Jehn et al., 2020), the [influence-effect](#) of climatic [factors-attributes](#) on streamflow indices [associated with rising and falling limbs](#) is [also finally studied/investigated here](#).

##### 46.1 Spatial Variability in Streamflow Indices

Streamflow indices related to rising limbs and falling limbs are computed for the selected catchments and displayed in spatial maps as shown in Fig. 5 and Fig. 6, respectively. The spatial analysis is based on the United States' geographical areas (for details, refer to Fig. 3b) as defined by NOAA's National Centers for Environmental Information and is referred to in the following spatial maps. Furthermore, ten clusters provided by Jehn et al. (2020) to represent the discrete hydrological behaviors of the continental United States are adopted in this study to understand the regional variability of catchment behavior. Figure [S2+](#) and Table [S2+](#) present the location map and details of the ten clusters.

337 For Section 4.1, the features/characteristics of the 10 clusters provided by Jehn et al. (2020) are used to interpret  
338 the findings of the results. Even though a comprehensive dataset like CAMELS provides an excellent overview  
339 of various catchments in contrasting climatic and topographic regions, it does not give conclusions to explain  
340 hydrologic behavior. facilitate an—and In order to address tackle this difficulty, we transformed the streamflow  
341 indices and presented them in clusters that represent distinct hydrological behavior which facilitates a ready the  
342 interpretation of hydrological processes. —easier—The ten clusters represent groups of catchments with distinct  
343 hydrological behavior and have distinct spatial patterns as well. The clusters presented by Jehn et al. (2020) are  
344 formed based on agglomerative hierarchical clustering with ward linkage on the principal components of the  
345 hydrological signatures. The hydrological signatures that are identified with the highest spatial predictability are  
346 used to cluster 643 catchments from the CAMELS dataset.

347 We first start by identifying the regions in the United States where high/low values of streamflow indices occur.  
348 The dominant catchment attributes of these identified—regions are also identified using corresponding clusters.  
349 Finally,—The streamflow indices and the dominant catchment attribute are then related to interpret the process  
350 behind the obtained findings. In terms of geographical regions, the rising limb density is highest over the Atlantic  
351 coast states, Ohio valley, Lower Mississippi Valley, Southern Great Plains, Southwest and Pacific, and lowest  
352 along the Upper Great Lakes region, Upper Mississippi Valley, Great Basin, and Northern Rocky Mountains,  
353 Northern Interior Plains, and East of Gulf Coast (Fig. 5.a). Further, in terms of hydrological clusters, Appalachian  
354 Mountains (Cluster 10), Southeastern and Central Plains (Cluster 1) and all Southern most states of the US (Cluster  
355 9) witness high rising limb densities and these clusters are characterized by a high forest fraction, low aridity, and  
356 high frequency of high precipitation events (Jehn et al., 2020), respectively (Fig. 6.a). The higher the forest  
357 proportion, the more precipitation is intercepted, resulting in a shallow rising limb and longer lag time of  
358 hydrograph. —A high frequency of high precipitation episodes, on the other hand, can result in more rising limbs  
359 and higher rising limb densities.

360 Northwestern Forested Mountains (Clusters 3, 4), located in the mountains of the western US, experience low  
361 values of rising limb density as these clusters are characterized by a dominant summer peak of discharge caused  
362 by rapid snowmelt (Fig. 6.a). In these clusters, we identified regions with low rising limb densities and the main  
363 catchment characteristics as dominant summer discharge peaks induced by quick snowmelt (Jehn et al., 2020). A  
364 long lag time and shallow rising limb might be caused by snow on the ground; hence low values of rising limbs  
365 might be caused by a longer lag time.

366 Considerably low values of rising limb scale parameters are experienced over the Rocky Mountains, High Plains,  
367 Great Plains, Upper Mississippi Valley, Great Basin, Southwest, and the Great Lakes regions, whereas the Pacific  
368 Northwest shows high values of rising limb scale parameters (Fig. 5.b). Clusters (5, 7) over the Northwestern  
369 Forested Mountains of CONUS experience very high values of rising limb scale parameters (Fig. 6.b). These  
370 catchments have the highest discharge, especially in the early summer, due to a combination of high precipitation  
371 and snowmelt. Further, the region in the Continental US which receives the highest precipitation is included in  
372 Cluster 5. Moreover, Cluster 5 consists of a large proportion of forest. Again, Cluster 7 with high values of rising  
373 limb scale parameter is characterized by high fraction of precipitation falling as snow. High precipitation and  
374 snowmelt might result in a large discharge. Higher discharges can create higher values of rising scale parameters  
375 as the rising limb scale parameter regulates the magnitude of the rising limb. Low values of rising limb scale

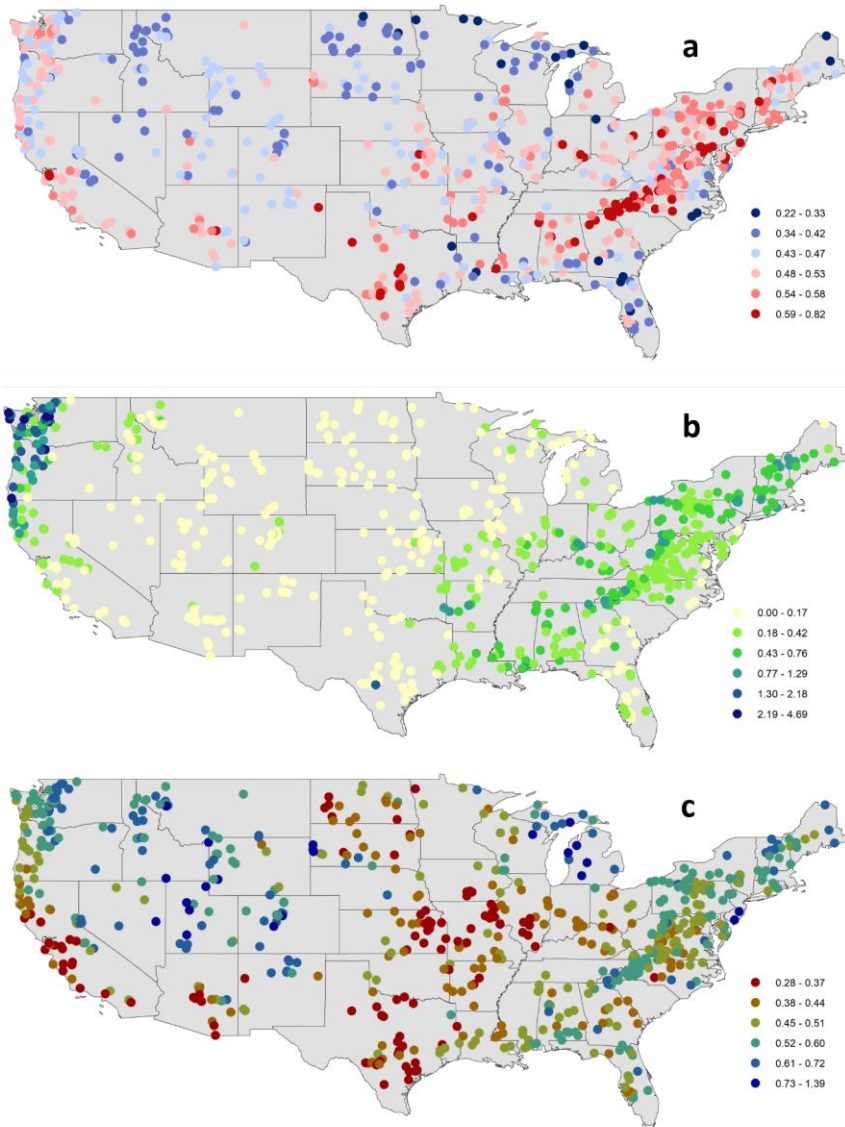
376 parameters are shown by Clusters 2, 8, 9. This is because of low water availability, low snow fraction precipitation  
377 falling as snow, and high evaporation experienced in these regions. Low discharge and thus lower rising limb  
378 scale parameters can be caused by excessive evaporation, low water availability, and a low snow fraction of  
379 precipitation falling as snow.

380 Low rising limb shape parameter occurs along the Great Plains, Mississippi Valley, Pacific coast, and the west of  
381 Gulf Coast (Fig. 5.c). In contrast, the shape parameter over the Rocky Mountains, High Plains, Great Basin, Pacific  
382 Northwest, and the Great Lakes region witnesses the highest values of rising limb shape parameters (Fig. 5.c). All  
383 the catchments located in the Southern states of the US (Cluster 9), Great Plains and North American deserts  
384 (Cluster 8), and the Central Plains (Cluster 2) characterize low values of rising limb shape parameters (Fig. 6.c).  
385 This is due to low water availability, low snow fraction precipitation falling as snow, low leaf area index, and high  
386 evaporation experienced in these regions. Excessive evaporation and a low snow fraction of precipitation falling  
387 as snow can contribute to low discharge and thus lower rising limb shape parameters. High values of rising limb  
388 shape parameters are seen in Clusters 3, 4 (Fig. 6.c) located in the Northwestern Forested Mountains of the western  
389 US, dominant with a summer peak of discharge caused by rapid snowmelt. The rapid snowmelt can cause flashy  
390 hydrographs with high values of rising limb shape parameters.

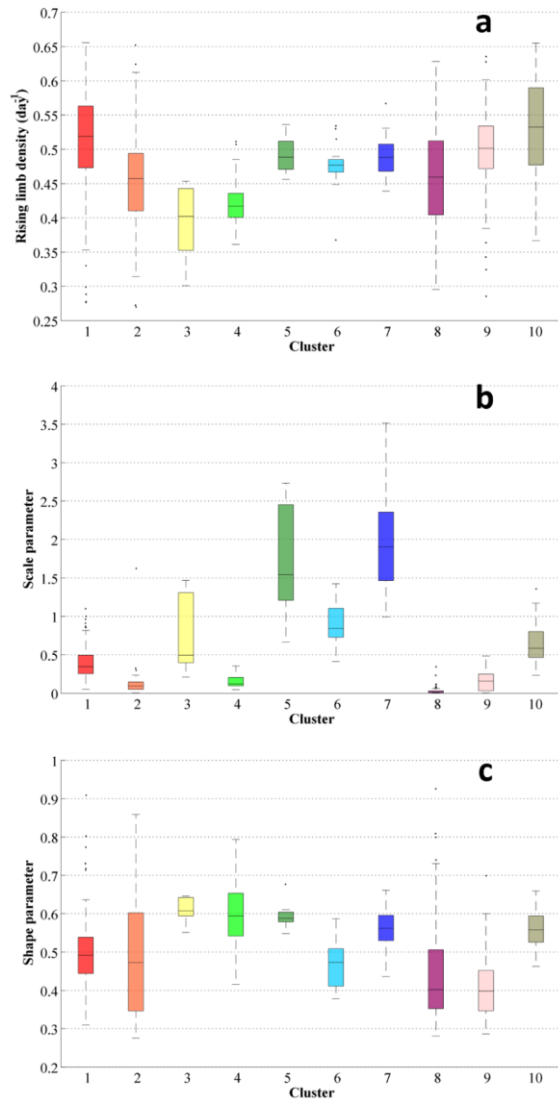
391 Catchments with a high falling limb density are predominantly located along the Great Basin and the Rocky  
392 Mountains and in the High Plains region (Fig. 7.a). Clusters 4, 2, 8 over Northwestern Forested Mountains, Central  
393 Plains, Great Plains, and North American deserts characterize higher magnitudes of falling limb density, and  
394 Clusters 6, 7 over Marine West Coast Forests and Western Cordillera smaller falling limb densities (Fig. 8.a).  
395 This is due to less presence of forest cover in these arid regions and -falling limb density shows a positive  
396 association with the arid climate.

397 Similarities exist between the patterns of the upper recession coefficient and the lower recession coefficient (Fig.  
398 7.b and Fig. 7.c). Clusters 3, 4 located in the Northwestern Forested Mountains, which have overall low discharge,  
399 show low values of upper and lower recession coefficients (Fig. 8.b and Fig. 8.c). Clusters 2, 9, located in the  
400 eastern US, witness high values of recession coefficients; due to low slope inclinations, water takes a long time  
401 to reach the outlet (Fig. 8.b and Fig. 8.c).





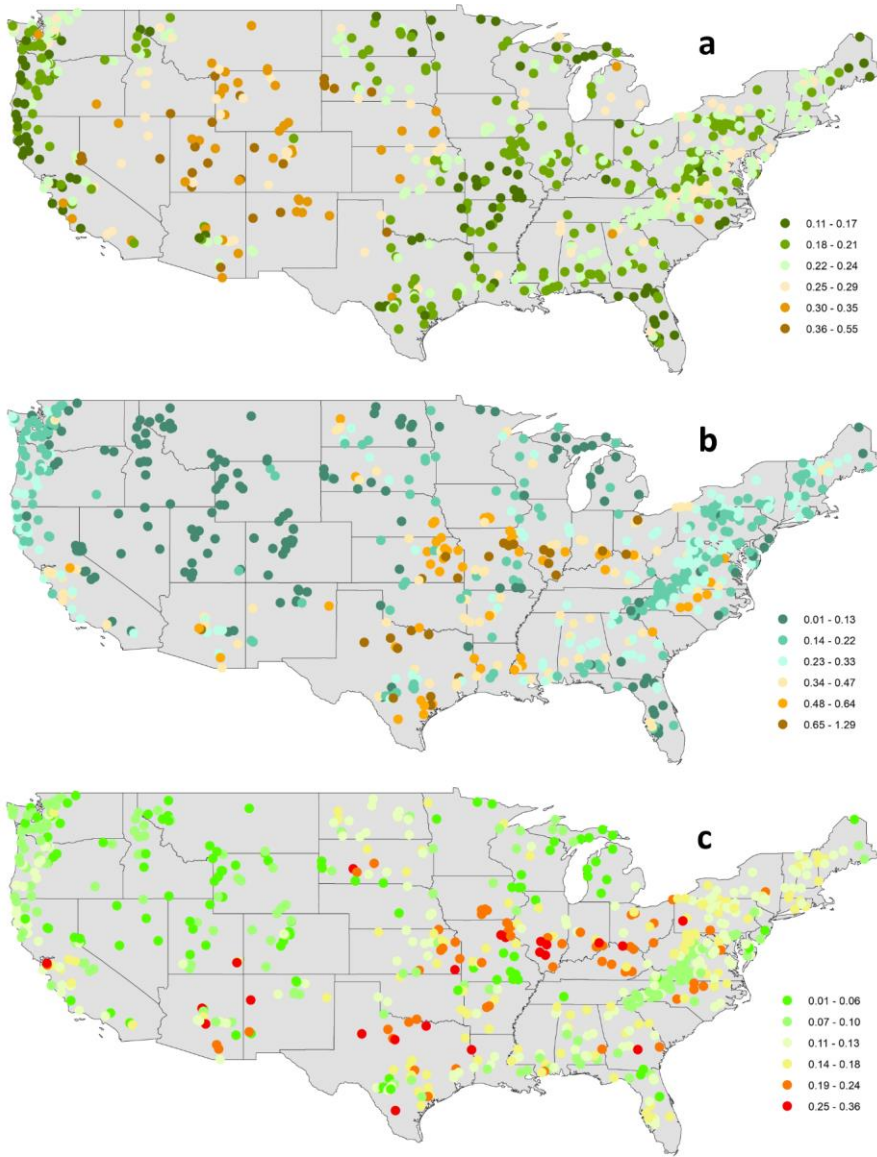
402  
 403 **Figure 5.** Spatial maps of streamflow indices associated with a rising limb (a) rising limb density [ $\text{day}^{-1}$ ], (b)  
 404 rising limb scale parameter, (c) rising limb shape parameter over the CONUS. ~~The Atlantic coast states, Ohio~~  
 405 ~~Valley, Lower Mississippi Valley, Southern Great Plains, Southwest, and Pacific have the highest rising limb~~  
 406 ~~density, while the Upper Great Lakes region, Upper Mississippi Valley, Great Basin, Northern Rocky Mountains,~~  
 407 ~~Northern Interior Plains, and East of Gulf Coast have the lowest. The Rocky Mountains, High Plains, Great Plains,~~  
 408 ~~Upper Mississippi Valley, Great Basin, Southwest, and Great Lakes regions have low values of rising limb scale~~  
 409 ~~parameters, but the Pacific Northwest has high values of rising limb scale parameters. The Great Plains,~~  
 410 ~~Mississippi Valley, Pacific coast, and west of Gulf Coast have low rising limb shape parameters. The shape~~  
 411 ~~parameter has the greatest values of rising limb shape parameters over the Rocky Mountains, High Plains, Great~~  
 412 ~~Basin, Pacific Northwest, and Great Lakes regions.~~



414

415 **Figure 6.** Boxplots of the hydrological descriptors linked with the rising limb (a) rising limb density [ $\text{day}^{-1}$ ], (b)  
 416 rising limb scale parameter, (c) rising limb shape parameter of the clusters over the CONUS. High rising limb  
 417 densities are observed in Clusters 10, 1, and 9, which are characterized by a high forest fraction, low aridity, and  
 418 a high frequency of high precipitation events, respectively. Rising limb scale parameters are exceptionally high  
 419 in Clusters 5, 7. Due to a combination of high precipitation and snowmelt, these catchments have the highest  
 420 discharge. Because of the low water availability, low snow fraction precipitation falling as snow, low leaf area  
 421 index, and high evaporation experienced in these areas, catchments in Cluster 9, Cluster 8, and Cluster 2 have low  
 422 values of rising limb shape parameters.

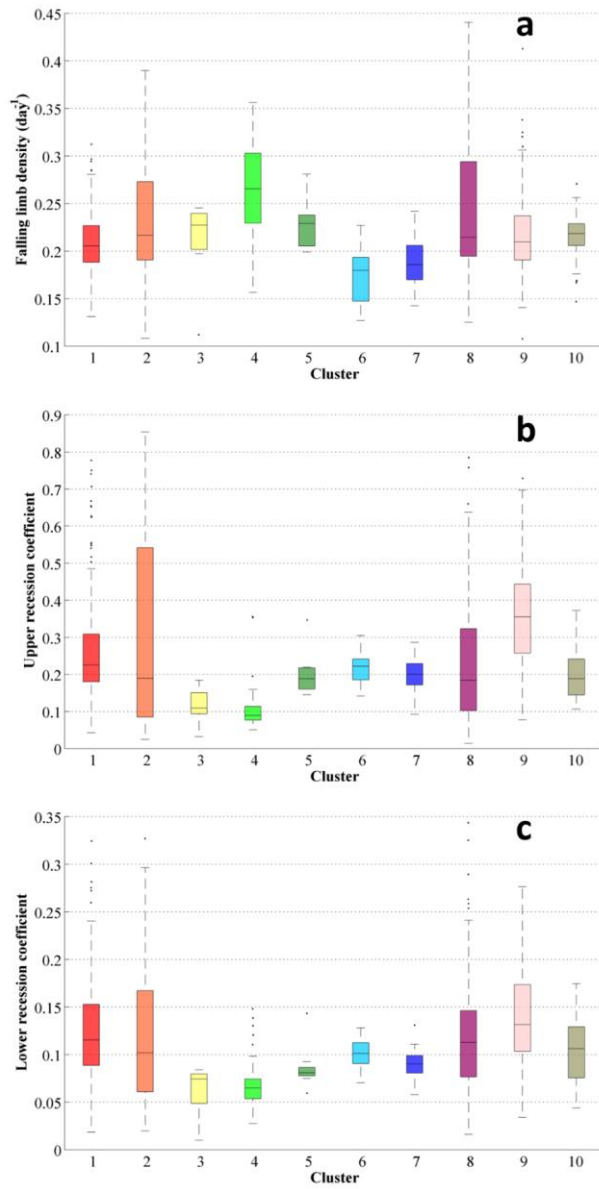
423



424

425 **Figure 7.** Regional variability of streamflow indices associated with the falling limb -(a) -falling limb density  
426 [day<sup>-1</sup>], (b) upper recession coefficient, (c) lower recession coefficient over the CONUS. **The Great Basin and the**  
427 **Rocky Mountains, and the High Plains region have high falling limb density. The patterns of the upper recession**  
428 **coefficient and the lower recession coefficient are similar.**

429



430

431 **Figure 8.** Boxplots of the streamflow indices related with the falling limb (a) falling limb density [ $\text{day}^{-1}$ ], (b)  
 432 upper recession coefficient, (c) lower recession coefficient of the clusters. Clusters 4, 2, 8 have higher falling limb  
 433 densities, while Clusters 6, 7 have lower falling limb densities due to the less forest cover in these arid areas.  
 434 Clusters 3, 4, which have a low discharge, have low upper and lower recession coefficients. Clusters 2, 9 have  
 435 high recession coefficients due to low slope inclinations.

436  
437  
438  
439  
440  
441  
442  
443  
444  
445  
446  
447  
448  
449  
450  
451  
452  
453  
454  
455  
456  
457  
458  
459  
460  
461  
462  
463  
464

#### 46.2 Relation of the Streamflow Indices ~~Flow Descriptors~~ and the Catchment Attributes

The association between the streamflow indices ~~flow descriptors~~ related to rising and falling limbs and catchment attributes is examined in this section. Table 23 shows the relation of streamflow indices linked with rising limb, and Table 34 shows the association of indices of the falling limb with catchment attributes. We used Spearman rank correlation for the correlation analysis. (in Tables 2 and 3). Green-colored coefficients represent positive correlation, and the red-colored correlation coefficients represent negative correlation. Table 2 and Table 3 have certain columns that are blank because only significant correlation values are provided in the table. Across all five attribute classes, the vegetation/land cover attributes positively correlate with all rising limb indices (Table 23). It can be seen that the rising limb density shows a positive correlation with all the three vegetation density indicators, namely fraction of forest, maximum leaf area index, maximum green vegetation fraction (Table 23).

However, it is observed that the rising limb scale parameter shows a negative correlation with climate and a positive association with the vegetation attributes (Table 23). Aridity and frequency of precipitation (Table 23) display a strong negative association with the rising limb scale parameter. It is noted that the rising limb shape parameter indicates a positive correlation with vegetation attributes and the fraction of precipitation falling as snow, mean slope, mean elevation, and sand fraction whereas, it negatively correlates with precipitation frequency.

Falling limb density is mainly governed by climate indices and is negatively correlated with the land cover characteristics (Table 34). Mean elevation also strongly characterizes the nature of the falling limb density. Besides, aridity and fraction of precipitation falling as snow are also positively correlated with falling limb density. Recession coefficients are negatively correlated with topographic indices (Table 34). Further, the recession coefficients show a positive correlation with clay and negative correlations with the fraction of precipitation falling as snow, forest fraction, and sand fraction. Moreover, the geology attributes such as subsurface porosity reveal a positive correlation to recession coefficients and a negative with subsurface permeability (Table 34).

465 **Table 23.** Correlation between streamflow indices linked with rising limb and the catchment attributes. Green  
 466 colored coefficients represent positive correlation, and the red-colored correlation coefficients represent the  
 467 negative correlation. **The vegetation/land cover attributes positively correlate with all rising limb indices amongst**  
 468 **all five attribute groups. It can be seen that the rising limb density has a positive relationship with all three**  
 469 **vegetation density measures. The rising limb scale parameter, has a negative association with climate and a**  
 470 **positive relationship with vegetation attributes. The rising limb shape parameter positively correlates with**  
 471 **vegetation attributes and the fraction of precipitation that falls as snow, mean slope, mean elevation, and sand**  
 472 **fraction.**

Spearman rank correlation coefficients	Topography			Climate						Soil			Land cover			Geology		
	Area	Mean elevation	Mean slope	Precipitation seasonality	Frac of precp as snow	Aridity	High precp freq	High precp dur	Low precp freq	Low precp dur	Depth to bedrock	Sand frac	Clay frac	Forest frac	LAI maximum	Green veg frac max	Subsurface porosity	Subsurface permeability
Shal	-	-	-	-	-	-	-	-	-	-	-	-	-	-	-	-	-	-
Scale	0.1	0.30	-	0.1	0.3	0.5	0.3	0.1	0.5	0.10	0.1	0.2	0.32	0.4	0.1	0.1	0.16	0.11
Rising	-	-	-	-	-	-	-	-	-	-	-	-	-	-	-	-	-	-
limb	0.4	-	-	0.1	0.20	0.3	0.3	0.3	0.3	0.08	0.4	0.5	0.15	0.4	0.6	0.2	0.2	0.2
density	0.3	0.3	0.3	0.3	0.3	0.3	0.3	0.3	0.3	0.3	0.3	0.3	0.3	0.3	0.3	0.3	0.3	0.3
parameters	0.6	0.5	0.5	0.6	0.5	0.6	0.5	0.6	0.5	0.6	0.5	0.6	0.5	0.6	0.5	0.6	0.5	0.6
ter	-	-	-	-	-	-	-	-	-	-	-	-	-	-	-	-	-	-
ity	-	-	-	-	-	-	-	-	-	-	-	-	-	-	-	-	-	-

Formatted: Font: 8 pt  
 Formatted: Indent: Left: 0 cm, Right: 0 cm  
 Formatted: Font: 8 pt  
 Formatted: Indent: Left: 0 cm, Right: 0 cm  
 Formatted: Font: 8 pt  
 Formatted: Indent: Left: 0 cm, Right: 0 cm

473  
 474  
 475  
 476  
 477  
 478  
 479  
 480  
 481  
 482  
 483  
 484  
 485  
 486  
 487  
 488  
 489  
 490

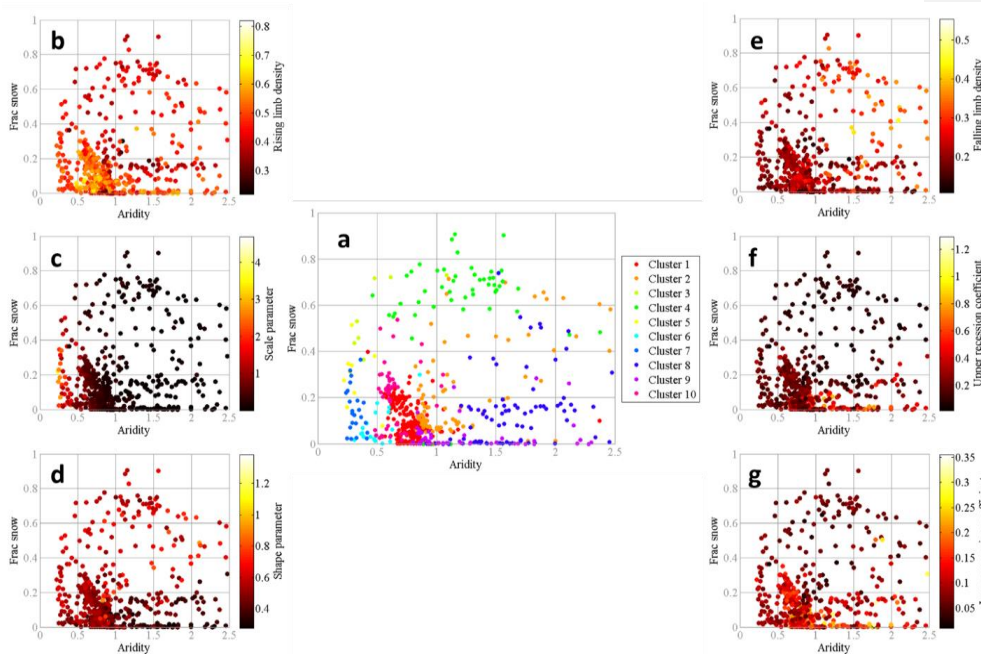
**Table 34.** Correlation between streamflow indices linked with falling limb and the catchment attributes. Green  
 colored coefficients represent positive correlation, and the red-colored correlation coefficients represent the  
 negative correlation. **Climate factors are the principal drivers of falling limb density and are negatively associated**  
 with land cover characteristics. **Topographic indicators are negatively correlated with recession coefficients.**  
 Furthermore, the recession coefficients reveal a positive association with clay and negative correlations with the  
 fraction of precipitation falling as snow, forest fraction, and sand fraction.

Spearman rank correlation coefficients	Topography	Climate	Soil	Land cover	Geology
--	------------	---------	------	------------	---------

Lower precipitation	0.13	Area
Falling limb density	0.55	Mean elevation
0.3	0.18	Mean slope
0.3	0.2	Precipitation seasonality
0.7	0.42	Frac of prec as snow
0.3	0.39	Aridity
0.2	0.3	High prec freq
0.1	0.12	High prec dur
0.1	0.2	Low prec freq
0.6	0.11	Low prec dur
0.2	0.1	Depth to bedrock
0.1	0.19	Sand frac
0.2	0.3	Clay frac
0.5	0.2	Forest frac
0.3	0.3	LAI maximum
0.17	0.0	Green veg frac max
0.37	0.40	Subsurface porosity
0.1	0.1	Subsurface permeability
0.6	0.3	
0.08	0.1	
0.0	0.0	

- Formatted: Font: 8 pt
- Formatted: Indent: Left: 0 cm, Right: 0 cm
- Formatted: Font: 8 pt
- Formatted: Indent: Left: 0 cm, Right: 0 cm
- Formatted: Font: 8 pt
- Formatted: Indent: Left: 0 cm, Right: 0 cm





492

493 **Figure 9.** (a) Comparison of the hydrological clusters of Jehn et al. (2020) with the climate index space (fraction of precipitation falling as snow vs. aridity). Single dots show the catchments and are colored by their hydrological clusters. Comparison of the streamflow indices in climate index space (b) rising limb density (c) rising limb scale parameter, (d) rising limb shape parameter, (e) falling limb density, (f) upper recession coefficient for all catchments. Single dots show the catchments and are colored according to the value of the streamflow indices. **Low values of rising limb density, high values of the rising limb shape parameter, and low values of recession coefficients are seen in catchments with a humid environment and a high fraction of precipitation falling as snow. In arid climates with a low fraction of precipitation falling as snow, the lowest values of rising limb scale and shape parameters, as well as the highest values of falling limb density, can be seen.**

502

503 **46.3 Influence of Attributes of Climate to Streamflow Indices** **Streamflow Indices with Attributes of Climate**

504 Climate attributes seem to be the most important indicator for hydrological behavior in the United States among the various attribute categories (Jehn et al., 2020). The climatic indices indicate a more substantial influence on hydrological signatures than the topographic, soil, land cover, and geological attributes combined (Addor et al., 2018). Additionally, the findings of Jehn et al. (2020) highlighted that the climate appears to be the most critical factor influencing hydrological behavior in the CAMELS dataset as a whole, and depending on the location, either aridity, snow, or seasonality are most important. Hence, the streamflow indices flow descriptors are then examined in the climate index space (aridity along x-axis and fraction of precipitation falling as snow along the y-axis) to evaluate the main drivers of the catchments. Single dots show the catchments and are colored by their hydrological clusters (Fig. 9.a).

513 Clusters 5, 6, 7, 1, 10 are characterized by a low fraction of precipitation falling as snow and humid climate, whereas Clusters 3, 4 have humid climate experiencing a high fraction of precipitation falling as snow (Fig. 9.a).

514

Formatted: English (India)



515 Clusters 2, 8, 9 are featured by a low fraction of precipitation falling as snow and arid climate (Fig. 9.a). The three  
516 categories mentioned above are referred to as G1, G2, and G3, respectively.

517 Clusters G1 with a low fraction of precipitation falling as snow with humid climate show (Clusters 1, 9, 10) high  
518 rising limb densities (Fig. 9.b) and (Clusters 5, 7) high rising limb scale parameters (Fig. 9.c). This is because the  
519 rising limb density negatively correlates with fraction of precipitation falling as snow (Fig. 9.b), whereas the rising  
520 limb scale parameter negatively correlates with aridity (Fig. 9.c). Moreover, these Clusters G1 experience a low  
521 value of (Clusters 6, 7) falling limb density (Fig. 9.e). This is because the falling limb density positively correlates  
522 with the climate indices (Fig. 9.e).

523 As mentioned earlier, Clusters G2 with humid climate and with a high fraction of precipitation falling as snow  
524 (Clusters 3, 4) display low values of rising limb density as rising limb density correlates negatively with the  
525 fraction of precipitation falling as snow (Fig. 9.b). G2 witnesses higher values of rising limb shape parameter due  
526 to its negative correlation with aridity and positive correlation with the fraction of precipitation falling as snow  
527 (Fig. 9.d). Furthermore, the Clusters of G2 (Clusters 3, 4) show low values of recession coefficients as they depict  
528 a strong negative correlation with the fraction of precipitation falling as snow (Fig. 9.f, g).

529 Low values of rising limb scale and shape parameters are noticed for the Clusters 2, 9, 8 (Clusters G3) with arid  
530 climate and low fraction of precipitation falling as snow (Fig. 9.c, d) due to its negative correlation with aridity as  
531 stated earlier. Cluster 8 experiences the maximum values of falling limb density (Fig. 9.e) where the region  
532 witnesses low fraction of snow and arid catchments, due to its strong positive correlates with the aridity.

### 533 **5.7 Concluding remarks**

534 Streamflow hydrograph portrays the time distribution of runoff at the point of measurement by a single curve, and  
535 the hydrographs are characterized by their time irreversibility property. In this study, the indices related to this  
536 characteristic feature are used to study the catchment drivers of streamflow hydrograph. The streamflow indices  
537 associated with the time irreversibility of hydrograph open new opportunities to investigate the interaction  
538 between topography, soil, climate, vegetation, geology that drive the hydrological behavior of catchments.  
539 Moreover, most of the previously presented hydrologic indices are employed only for time-symmetric processes  
540 (McMillan, 2021); the importance of the time irreversibility of streamflow is highlighted in this study. The indices  
541 associated with rising and falling limbs are primarily correlated to distinct catchment attributes, establishing a  
542 relationship between the indices and catchment attributes such as climate, topography, soil, geology, and  
543 vegetation to delineate the controlling drivers in corresponding hydrograph sections. A set of streamflow indices  
544 with temporal asymmetry for 671 catchments in the United States is presented in this study. The regional  
545 variations among catchments over the United States are compared and discussed using the spatial maps of  
546 streamflow indices. Such spatial maps of the streamflow indices supplement the hydrometeorological time series  
547 and catchment attributes provided by Addor et al. (2017).

548 The study revealed that the rising limb indices such as rising limb density, rising limb shape parameter and rising  
549 limb scale parameter correlate positively with vegetation indices. Falling limb density is primarily controlled by  
550 climate indices and is negatively correlated with land cover characteristics; the structure of the falling limb density  
551 is also closely influenced by mean elevation. Finally, [streamflow indices](#) ~~flow descriptors~~ are studied in the climate  
552 index space to isolate the runoff generation's leading drivers. High rising limb densities and rising limb scale

553 parameters are observed in catchments with low precipitation falling as snow and a humid climate. It is observed  
554 that the catchments with a humid climate and a high fraction of precipitation falling as snow display low values  
555 of rising limb density, high values of the rising limb shape parameter, and low values of recession coefficients.  
556 The lowest values of rising limb scale and shape parameters, and the highest values of falling limb density, are  
557 seen in catchments of arid climates and a low fraction of precipitation falling as snow.

558 In general, the contribution of this work lies in differentiating hydrographs depending on their time irreversibility  
559 property and using the corresponding indices to provide an alternative methodology for identifying the drivers of  
560 streamflow hydrographs. In the context of large-sample hydrology research, the concept of time-irreversibility  
561 and the indices associated with it could also be used to describe the drivers at catchment scale.

562

563 *Data availability.* The CAMELS dataset can be found at <https://doi.org/10.5194/hess21-5293-2017> (Addor et al.  
564 2017).

565 *Competing interests.* The authors declare that they have no conflict of interest.

566 *Acknowledgements.* We would like to thank all the people who created the CAMELS dataset. The funding  
567 received from the Ministry of Earth Sciences (MoES), Government of India, through the project, “Advanced  
568 Research in Hydrology and Knowledge Dissemination”, Project No.: MOES/PAMC/H&C/41/2013-PC-II, is  
569 gratefully acknowledged.

570

## 571 **References**

572

573 Addor, Newman, A. J., Mizukami, N. and Clark, M. P.: The CAMELS data set: catchment attributes and  
574 meteorology for large-sample studies, *Hydrol. Earth Syst. Sci.*, 21(10), 5293–5313, doi:10.5194/hess-21-5293-  
575 2017, 2017.

576 Addor, Nearing, G., Prieto, C., Newman, A. J., Le Vine, N. and Clark, M. P.: A Ranking of Hydrological  
577 Signatures Based on Their Predictability in Space, *Water Resour. Res.*, 54(11), 8792–8812,  
578 doi:10.1029/2018WR022606, 2018.

579 Addor, N., Do, H. X., Alvarez-Garreton, C., Coxon, G., Fowler, K. and Mendoza, P. A.: Large-sample hydrology:  
580 recent progress, guidelines for new datasets and grand challenges, *Hydrol. Sci. J.*, 65(5), 712–725,  
581 doi:10.1080/02626667.2019.1683182, 2020.

582 Alvarez-Garreton, C., Mendoza, P. A., Pablo Boisier, J., Addor, N., Galleguillos, M., Zambrano-Bigiarini, M.,  
583 Lara, A., Puelma, C., Cortes, G., Garreaud, R., McPhee, J. and Ayala, A.: The CAMELS-CL dataset: Catchment  
584 attributes and meteorology for large sample studies-Chile dataset, *Hydrol. Earth Syst. Sci.*, 22(11), 5817–5846,  
585 doi:10.5194/hess-22-5817-2018, 2018a.

586 Alvarez-Garreton, C., Mendoza, P. A., Boisier, J. P., Addor, N., Galleguillos, M., Zambrano-Bigiarini, M., Lara,  
587 A., Puelma, C., Cortes, G., Garreaud, R., McPhee, J. and Ayala, A.: The CAMELS-CL dataset: catchment  
588 attributes and meteorology for large sample studies – Chile dataset, *Hydrol. Earth Syst. Sci.*, 22(11), 5817–5846,  
589 doi:10.5194/hess-22-5817-2018, 2018b.

590 Arsenault, R., Bazile, R., Ouellet Dallaire, C. and Brissette, F.: CANOPEX: A Canadian hydrometeorological  
591 watershed database, *Hydrol. Process.*, 30(15), 2734–2736, doi:10.1002/hyp.10880, 2016.

592 Berghuijs, W. R., Sivapalan, M., Woods, R. A. and Savenije, H. H. G.: Patterns of similarity of seasonal water  
593 balances: A window into streamflow variability over a range of time scales, *Water Resour. Res.*, 50(7), 5638–  
594 5661, doi:10.1002/2014WR015692, 2014.

595 Blöschl, G., Hall, J., Viglione, A., Perdigão, R. A. P., Parajka, J., Merz, B., Lun, D., Arheimer, B., Aronica, G.  
596 T., Bilibashi, A., Boháč, M., Bonacci, O., Borga, M., Čanjevac, I., Castellarin, A., Chirico, G. B., Claps, P.,  
597 Frolova, N., Ganora, D., Gorbachova, L., Gül, A., Hannaford, J., Harrigan, S., Kireeva, M., Kiss, A., Kjeldsen, T.  
598 R., Kohnová, S., Koskela, J. J., Ledvinka, O., Macdonald, N., Mavrova-Guirguinova, M., Mediero, L., Merz, R.,  
599 Molnar, P., Montanari, A., Murphy, C., Osuch, M., Ovcharuk, V., Radevski, I., Salinas, J. L., Sauquet, E., Šraj,  
600 M., Szolgay, J., Volpi, E., Wilson, D., Zaimi, K. and Živković, N.: Changing climate both increases and decreases  
601 European river floods, *Nature*, 573(7772), 108–111, doi:10.1038/s41586-019-1495-6, 2019.

602 Clark, M. P., McMillan, H. K., Collins, D. B. G., Kavetski, D. and Woods, R. A.: Hydrological field data from a  
603 modeller’s perspective: Part 2: Process-based evaluation of model hypotheses, *Hydrol. Process.*, 25(4), 523–543,  
604 doi:10.1002/hyp.7902, 2011.

605 Coxon, G., Freer, J., Wagener, T., Odoni, N. A. and Clark, M.: Diagnostic evaluation of multiple hypotheses of  
606 hydrological behaviour in a limits-of-acceptability framework for 24 UK catchments, *Hydrol. Process.*, 28(25),  
607 6135–6150, doi:10.1002/hyp.10096, 2014.

608 Coxon, G., Addor, N., Bloomfield, J. P., Freer, J., Fry, M., Hannaford, J., Howden, N. J. K., Lane, R., Lewis, M.,  
609 Robinson, E. L., Wagener, T. and Woods, R.: CAMELS-GB: hydrometeorological time series and landscape  
610 attributes for 671 catchments in Great Britain, *Earth Syst. Sci. Data*, 12(4), 2459–2483, doi:10.5194/essd-12-  
611 2459-2020, 2020.

612 Do, H. X., Gudmundsson, L., Leonard, M. and Westra, S.: The Global Streamflow Indices and Metadata Archive  
613 (GSIM) – Part 1: The production of a daily streamflow archive and metadata, *Earth Syst. Sci. Data*, 10(2), 765–  
614 785, doi:10.5194/essd-10-765-2018, 2018.

615 Duan, Q., Schaake, J., Andréassian, V., Franks, S., Goteti, G., Gupta, H. V., Gusev, Y. M., Habets, F., Hall, A.,  
616 Hay, L., Hogue, T., Huang, M., Leavesley, G., Liang, X., Nasonova, O. N., Noilhan, J., Oudin, L., Sorooshian,  
617 S., Wagener, T. and Wood, E. F.: Model Parameter Estimation Experiment (MOPEX): An overview of science  
618 strategy and major results from the second and third workshops, *J. Hydrol.*, 320(1–2), 3–17,  
619 doi:10.1016/j.jhydrol.2005.07.031, 2006.

620 Ehret, U., Gupta, H. V., Sivapalan, M., Weijs, S. V., Schymanski, S. J., Blöschl, G., Gelfan, A. N., Harman, C.,  
621 Kleidon, A., Bogaard, T. A., Wang, D., Wagener, T., Scherer, U., Zehe, E., Bierkens, M. F. P., Di Baldassarre,  
622 G., Parajka, J., van Beek, L. P. H., van Griensven, A., Westhoff, M. C. and Winsemius, H. C.: Advancing  
623 catchment hydrology to deal with predictions under change, *Hydrol. Earth Syst. Sci.*, 18(2), 649–671,  
624 doi:10.5194/hess-18-649-2014, 2014.

625 Ghiggi, G., Humphrey, V., Seneviratne, S. I. and Gudmundsson, L.: GRUN: an observation-based global gridded  
626 runoff dataset from 1902 to 2014, *Earth Syst. Sci. Data*, 11(4), 1655–1674, doi:10.5194/essd-11-1655-2019, 2019.

627 Gudmundsson, L., Do, H. X., Leonard, M. and Westra, S.: The Global Streamflow Indices and Metadata Archive

628 (GSIM) – Part 2: Quality control, time-series indices and homogeneity assessment, *Earth Syst. Sci. Data*, 10(2),  
629 787–804, doi:10.5194/essd-10-787-2018, 2018.

630 Gupta, H. V., Perrin, C., Blöschl, G., Montanari, A., Kumar, R., Clark, M. and Andréassian, V.: Large-sample  
631 hydrology: a need to balance depth with breadth, *Hydrol. Earth Syst. Sci.*, 18(2), 463–477, doi:10.5194/hess-18-  
632 463-2014, 2014.

633 Jehn, F. U., Bestian, K., Breuer, L., Kraft, P. and Houska, T.: Using hydrological and climatic catchment clusters  
634 to explore drivers of catchment behavior, *Hydrol. Earth Syst. Sci.*, 24(3), 1081–1100, doi:10.5194/hess-24-1081-  
635 2020, 2020.

636 [Khrystyuk, B., Gorbachova, L. and Koshkina, O.: The impact of climatic conditions of spring flood formation  
637 on hydrograph shape of the Desna River, \*Meteorol. Hydrol. Water Manag.\*, 5\(1\), 63–70,  
638 doi:10.26491/mhwm/67914, 2017.](#)

639 Koutsoyiannis, D.: Simple stochastic simulation of time irreversible and reversible processes, *Hydrol. Sci. J.*,  
640 doi:10.1080/02626667.2019.1705302, 2020.

641 Kuentz, A., Arheimer, B., Hundecha, Y. and Wagener, T.: Understanding hydrologic variability across Europe  
642 through catchment classification, *Hydrol. Earth Syst. Sci.*, 21(6), 2863–2879, doi:10.5194/hess-21-2863-2017,  
643 2017.

644 Linke, S., Lehner, B., Ouellet Dallaire, C., Ariwi, J., Grill, G., Anand, M., Beames, P., Burchard-Levine, V.,  
645 Maxwell, S., Moidu, H., Tan, F. and Thieme, M.: Global hydro-environmental sub-basin and river reach  
646 characteristics at high spatial resolution, *Sci. Data*, 6(1), 283, doi:10.1038/s41597-019-0300-6, 2019.

647 Mathai and Mujumdar, P. P.: Multisite Daily Streamflow Simulation With Time Irreversibility, *Water Resour.*  
648 *Res.*, 55(11), 9334–9350, doi:10.1029/2019WR025058, 2019.

649 McMillan, H. K.: A review of hydrologic signatures and their applications, *WIREs Water*, 8(1), 1–23,  
650 doi:10.1002/wat2.1499, 2021.

651 McMillan, H. K., Clark, M. P., Bowden, W. B., Duncan, M. and Woods, R. A.: Hydrological field data from a  
652 modeller's perspective: Part 1. Diagnostic tests for model structure, *Hydrol. Process.*, 25(4), 511–522,  
653 doi:10.1002/hyp.7841, 2011.

654 Newman, A. J., Clark, M. P., Sampson, K., Wood, A., Hay, L. E., Bock, A., Viger, R. J., Blodgett, D., Brekke,  
655 L., Arnold, J. R., Hopson, T. and Duan, Q.: Development of a large-sample watershed-scale hydrometeorological  
656 data set for the contiguous USA: data set characteristics and assessment of regional variability in hydrologic model  
657 performance, *Hydrol. Earth Syst. Sci.*, 19(1), 209–223, doi:10.5194/hess-19-209-2015, 2015.

658 Richter, B. D., Baumgartner, J. V., Powell, J. and Braun, D. P.: A Method for Assessing Hydrologic Alteration  
659 within Ecosystems, *Conserv. Biol.*, 10(4), 1163–1174, doi:10.1046/j.1523-1739.1996.10041163.x, 1996.

660 [Roberts, M. C. and Klingeman, P. C.: The influence of landform and precipitation parameters on flood  
661 hydrographs, \*J. Hydrol.\*, 11\(4\), 393–411, doi:10.1016/0022-1694\(70\)90004-1, 1970.](#)

662 [Rogers, W. F.: New concept in hydrograph analysis, \*Water Resour. Res.\*, 8\(4\), 973–981,  
663 doi:10.1029/WR008i004p00973, 1972.](#)

Formatted: Left, Space Before: 6 pt, After: 6 pt

Formatted: Font: Do not check spelling or grammar

Formatted: Left, Space Before: 6 pt, After: 6 pt

Formatted: Font: Do not check spelling or grammar

664 Sawicz, K., Wagener, T., Sivapalan, M., Troch, P. A. and Carrillo, G.: Catchment classification : empirical  
665 analysis of hydrologic similarity based on catchment function in the eastern USA, *Hydrol. Earth Syst. Sci.*, 8(3),  
666 2895–2911, doi:10.5194/hess-15-2895-2011, 2011.

667 Sawicz, K. A., Kelleher, C., Wagener, T., Troch, P., Sivapalan, M. and Carrillo, G.: Characterizing hydrologic  
668 change through catchment classification, *Hydrol. Earth Syst. Sci.*, 18(1), 273–285, doi:10.5194/hess-18-273-  
669 2014, 2014.

670 Serinaldi, F. and Kilsby, C. G.: Irreversibility and complex network behavior of stream flow fluctuations, *Phys.*  
671 *A Stat. Mech. its Appl.*, 450, 585–600, doi:10.1016/j.physa.2016.01.043, 2016.

672 Shamir, E., Imam, B., Morin, E., Gupta, H. V. and Sorooshian, S.: The role of hydrograph indices in parameter  
673 estimation of rainfall-runoff models, *Hydrol. Process.*, 19(11), 2187–2207, doi:10.1002/hyp.5676, 2005.

674 [Singh, V. P.: Effect of spatial and temporal variability in rainfall and watershed characteristics on stream flow](#)  
675 [hydrograph, \*Hydrol. Process.\*, 11\(12\), 1649–1669, doi:10.1002/\(SICI\)1099-1085\(19971015\)11:12<1649::AID-  
676 HYP495>3.0.CO;2-1, 1997.](#)

677 Stagge, J. H. and Moglen, G. E.: A nonparametric stochastic method for generating daily climate-adjusted  
678 streamflows, *Water Resour. Res.*, 49, 6179–6193, doi:10.1002/wrcr.20448, 2013.

679 Szilagyi, J., Balint, G. and Csik, A.: Hybrid, Markov chain-based model for daily streamflow generation at  
680 multiple catchment sites, *J. Hydrol. Eng.*, 11(3), 245–256, 2006.

681

682

Formatted: Left, Space Before: 6 pt, After: 6 pt

Formatted: Font: Do not check spelling or grammar